Optical Society of America. Michael L. Basehore and Daniel Post, "Displacement fields (U,W) obtained simultaneously by moiré interferometry," Appl. Opt. 21, 2558-2562 (1982). doi: 10.1364/AO.21.002558

Displacement fields (U, W) obtained simultaneously by moiré interferometry

Michael L. Basehore and Daniel Post

A high-frequency phase grating on a specimen surface is illuminated symmetrically by two oblique beams. The diffracted beams emerge with wave front warpages that define both the in-plane U and out-of-plane W displacement fields. Contour maps of these wave fronts, with added carrier fringes, are obtained as a single photographic record. They are manipulated by moiré and optical filtering steps to yield whole-field fringe patterns of U and W. Sensitivities of 0.833 μm/fringe (32.8 μin./fringe) for in-plane displacements and 0.132 μm/fringe (5.2 μin./fringe) for out-of-plane displacements were demonstrated. Since data acquisition is experimentally simple, dynamic as well as static analyses are applicable.

I. Introduction

In an earlier investigation, we prepared the foundation for the current work.[1] Prescribing the normal arrangement of moiré interferometry (Fig. 1), we showed that the two wave fronts emerging from a deformed specimen grating can be used to determine not only the in-plane displacement but out-of-plane displacements as well. In this previous work, holographic interferometry was used to capture the wave front contours. Subsequent addition and subtraction of the resulting parametric data led to out-of-plane and in-plane displacements, respectively.

The present work is intended to provide a technique where both addition and subtraction are performed automatically by optical moiré methods. The objective is to extract two distinct fringe patterns: (1) a contour map of in-plane displacements U or V (depicting the x- or y-displacement field, respectively) and (2) a contour map of out-of-plane displacements W (representing the z-displacement field).

In Fig. 1, two mutually coherent beams A and B intersect at angle 2α to form a virtual grating[2] of frequency f lines/mm, where

$$f = (2/\lambda)\sin\alpha \tag{1}$$

and where λ is the wavelength of the light. When the frequency of the diffraction grating on the specimen is $f/2$, light diffracted in the +1 order from beam A and the -1 order from beam B emerges normal to the specimen. Ideally both beams have coincident plane wave fronts, indicated by line $A'B'$ in Fig. 1. When the specimen is deformed and displaced by external forces, the attached specimen grating is deformed and displaced too. Therefore, angles of diffraction change slightly, but systematically, at each point in the grating, and the two previously plane wave fronts become warped wave fronts A'' and B''.

Let λN_a represent the separation between warped wave front A'' and its original plane $A'B'$. Let λN_b represent the separation between warped wave front B'' and $A'B'$. Reference 1 shows that in-plane displacements of the specimen grating result in symmetrically opposite warpages of these wave fronts; i.e., $N_a = -N_b$, while out-of-plane displacements cause wave fronts A and B to experience equal warpages, i.e., $N_a = N_b$. Thus $N_a - N_b$ is a unique measure of in-plane displacements, while $N_a + N_b$ is a unique measure of out-of-plane displacements.

These parameters determine the U and W displacements of the specimen surface by[1]

$$U = (1/f)(N_a - N_b), \tag{2}$$

$$W = \frac{\lambda}{2(1+\cos\alpha)}(N_a + N_b). \tag{3}$$

Here f is the virtual grating frequency given by Eq. (1), and grating lines are initially perpendicular to the x direction. Of course, if the grating lines are initially perpendicular to the y direction, in-plane displacement V would be determined as well as redundant W data.

The subtractive parameter, $N_a - N_b$, is also recognized as the fringe order N of in-plane moiré interferometry techniques,[3] where $U = (1/f)N$. Consequently the means to generate the fringe pattern corresponding to the additive parameter, $N_a + N_b$, is of primary interest.

When this work was done both authors were with Virginia Polytechnic Institute & State University, Engineering Science & Mechanics Department, Blacksburg, Virginia 24061; Michael Basehore is now with Battelle-Columbus Laboratories, Columbus, Ohio 43201.

Received 8 January 1982.
0003-6935/82/142558-05$01.00/0.

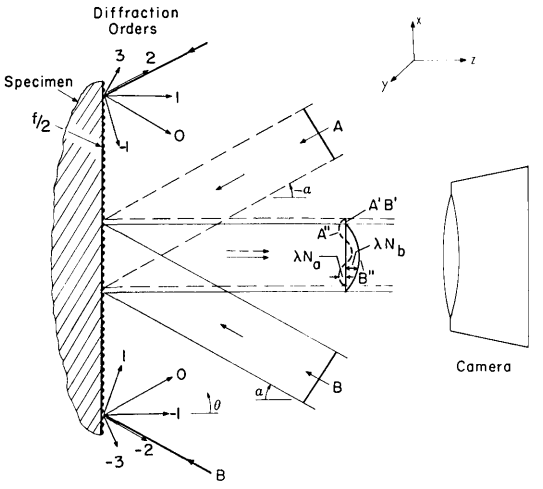

Fig. 1. Symmetric arrangement of moiré interferometry.

The basic plan is to generate interference patterns that are contour maps of N_a and N_b but with added carrier patterns of opposite signs. As a result of the negative carrier, superposition of these two patterns produces additive moiré fringes yielding $N_a + N_b$ instead of the more familiar subtractive moiré. The following sections describe two experimental techniques that can be used.

Numerous moiré and holographic techniques for out-of-plane displacement measurements appear in the literature. Two that relate to this work are Refs. 4 and 5.

II. Experimental Apparatus

The experimental arrangement is illustrated in Fig. 2. It is the same apparatus as described in Refs. 3 and 6 except for addition of the auxiliary mirror. The auxiliary mirror is uncoated, but it has a dielectric reflectance of ~4%; it is slightly wedge-shaped so the reflection from its rear surface emerges in a different direction and can be disregarded. When the frequency of the specimen grating is precisely one-half of the frequency of the virtual reference grating and the lines of the specimen grating are exactly parallel to the lines of the virtual grating, emerging beams a, b, and o (depicted here as rays) are coincident. However, when the frequency of the virtual grating is changed by slightly decreasing angle α, active beams a and b deviate slightly by symmetrically opposite angles with respect to auxiliary beam o, as shown. This divergence of beams produces a carrier pattern of extension.

Alternatively, let emerging rays a, b, and o be coincident again but rotate the specimen slightly about an axis normal to its surface. Active rays a and b will then emerge with angular deviations essentially as shown, but they will spread apart in the plane perpendicular to the page instead of in the page. This produces a carrier pattern of rotation. In either case, when the three beams are intercepted by a lens as illustrated in Fig. 3, they are converged to three distinct locations on the camera aperture plate.

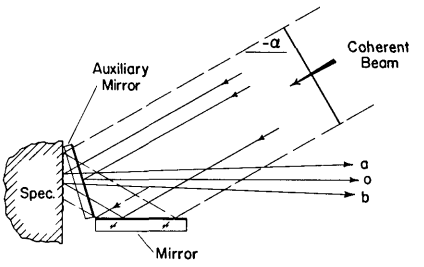

Fig. 2. Experimental arrangement. The full mirror generates a symmetrical input beam at angle $+\alpha$, and the auxiliary partial mirror provides auxiliary beam o.

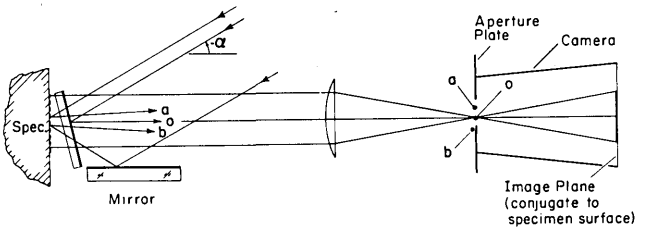

Fig. 3. Beams represented by rays a, b, and o converge to different points on the camera aperture plate.

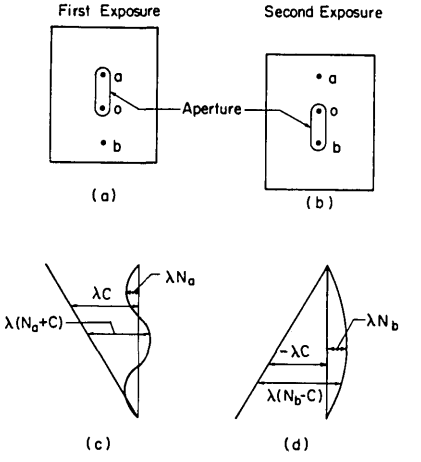

Fig. 4. In Scheme I, two beams and their corresponding wave fronts are admitted into the camera for each exposure.

III. Scheme I

The additive quality can be manifest in the following manner. Let the aperture plate of Fig. 3 be positioned to allow light from beams a and o to enter the camera [Fig. 4(a)] for a first exposure. Reposition the aperture to allow light from beams b and o to enter the camera [Fig. 4(b)] for a second exposure on the same film. With the aid of Fig. 4(c), it can be seen that interference of beams a and o produces a contour map of $N_a + C$. Here C represents the uniform contours of a carrier pattern caused by the angular deviation between beams a and o, and N_a represents the contours of warped wave front **a** or A''. Similarly interference between beams b and o produces a contour map of $N_b - C$ as shown in Fig. 4(d). This carrier pattern is designated as $-C$,

since the angular deviation of beams b and o is opposite that between beams a and o.

With the lens (Fig. 3) adjusted to focus an image of the specimen surface on the camera back, the two patterns are coincident. This superposition of interference patterns $N_a + C$ and $N_b - C$ on the same negative creates a moiré pattern. It is well known that both additive and subtractive fringes exist simultaneously in a moiré pattern, although only one has good visibility.[7] The additive moiré consists of a family whose fringe orders N' are defined as the sum of the fringe orders of the superimposed patterns, which in the present case is

$$N' = (N_a + C) + (N_b - C) = N_a + N_b. \quad (4)$$

The subtractive moiré consists of lines whose fringe orders N are defined as the difference of the fringe orders of the superimposed patterns, or

$$N = (N_a + C) - (N_b - C) = N_a - N_b + 2C. \quad (5)$$

Since the angular deviations between beams a and o and between b and o yield carrier patterns C of high frequency (e.g., 20 fringes/mm), N consists of very closely spaced fringes in which the moiré phenomenon is not visible. In this case, the additive moiré yields coarser visible fringes of $N_a + N_b$. This is the desired pattern, from which out-of-plane displacements are determined by Eq. (3).

The in-plane displacement field can also be obtained. For this, beam o is blocked, and light from beams a and b is allowed to enter the camera aperture simultaneously. A no-load exposure is made resulting in an interference pattern of $N_i = (N_a - N_b + 2C)_i$. The specimen is loaded, and a second exposure is made on the same film, this one depicting $N_p = (N_a - N_b + 2C)_p$. Subscripts i and p denote the initial or no-load condition and the full-load condition, respectively. These superimposed patterns combine to form a moiré pattern of their difference, namely $N = (N_a - N_b)_{p-i}$. The fringes show the load-induced pattern of $N_a - N_b$ uniquely, since the initial or no-load contribution is canceled. Of course, this yields in-plane displacements by Eq. (2).

A. Optical Filtering I

The patterns of out-of-plane and in-plane displacements are moiré patterns obtained by double exposure. Such moiré fringes have inherently low contrast, but they can be transformed to patterns of excellent contrast by optical filtering.[3,6] The apparatus illustrated in Fig. 5 is used with the double-exposure film (or negative) placed as shown. The negative is photographed by admitting light of one nonzero diffraction order into the camera, and the result is a high-contrast rendition of the moiré pattern, like those of Fig. 8.

IV. Scheme II

Although the technique described above is capable of yielding both the in-plane and out-of-plane displacement fields, two qualities can be enhanced. In Scheme I,

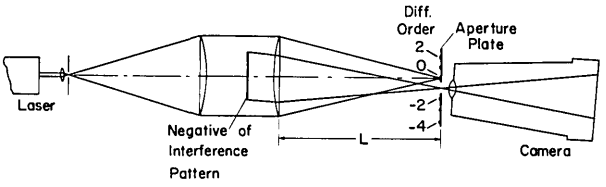

Fig. 5. Arrangement for optical filtering. Of the many beams diffracted by the negative, one or two selected beams are allowed to pass through the aperture plate.

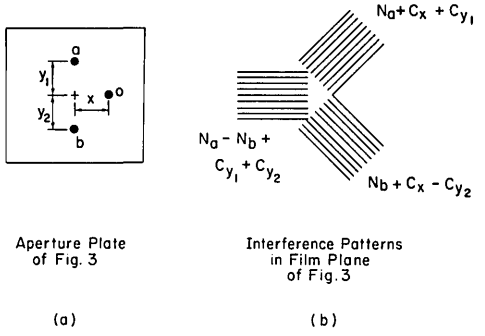

Fig. 6. In Scheme II, all three beams are allowed to pass simultaneously through the aperture plate of Fig. 3 to produce the three superimposed fringe patterns illustrated in (b).

(1) the double exposure required in the load condition precludes transient dynamic investigations;

(2) if the W displacement field for the no-load condition exhibits fringes, their fringe orders must be subtracted manually to determine the load-induced W field.

Scheme II provides an alternative that circumvents these drawbacks.

The basic plan uses carrier patterns too, but here they are not parallel to the coordinate axes. The y components of the carrier patterns have opposite signs, and their x components have the same sign. The opposite carriers permit extraction of the additive moiré parameter, while the carriers with a common sign provide for subsequent subtraction of the load and no-load patterns.

The same experimental arrangement (Fig. 3) is utilized. However, the auxiliary mirror is rotated to deviate beam o. The positions of the three beams converged to the camera aperture plate are illustrated in Fig. 6(a). It should be noted that the distances identified as y_1, y_2, and x on Fig. 6(a) are not exacting quantities that require precision adjustments. Indeed it is not even necessary that $y_1 = y_2$ for this scheme, although for later operations it is convenient if $y_1 \approx y_2 \approx x$. The only requirement is that they remain constant for both the no-load and load exposures described in the following sections.

Light from all three beams is allowed to enter the camera, resulting in three superimposed interference patterns depicted in Fig. 6(b). When the specimen is loaded and wave fronts A'' and B'' become warped, these patterns represent

(1) interference between beams a and o producing

a contour map of $N_a + C_x + C_{y1}$ (once again N_a represents the contours of warped wave front a, or A'', while C_x and C_{y1} are components of a carrier pattern caused by orthogonal angular deviations between beams a and o);

(2) interference between beams b and o producing a contour map of $N_b + C_x - C_{y2}$;

(3) interference between beams a and b resulting in a contour map of $N_a + C_{y1} - (N_b - C_{y2})$ or $N_a - N_b + C_{y1} + C_{y2}$.

Although shown separately in Fig. 6(b), the three interference patterns are in fact superimposed over the entire image. It will be shown that this single photographic record, combined with a corresponding no-load pattern, provides $N_a - N_b$ and $N_a + N_b$. Optical filtering is used to extract the information.

A. Optical Filtering II

An optical filtering technique, again using the apparatus of Fig. 5, can be used to isolate the warped wave fronts in such a manner that they may be judiciously recombined to yield the subtractive and additive parameters. A photographic film is exposed in the moiré interferometry system and developed. The resulting photographic negative contains the three interference patterns described above. In each the carrier pattern is dominant, with wave front warpage information manifest as irregularities in the otherwise uniform carriers. When placed in the optical filtering system illustrated in Fig. 5, each of the three patterns behaves as a coarse diffraction grating. Beams emerge from the negative in the various directions of the diffraction orders of the three carrier gratings and are converged to separate points on the aperture plate of Fig. 5. Figure 7 portrays the array of bright spots of light seen on the plate. Although shown here as distinct points of light, they are in fact local clouds of points. The information that each of the beams carries, i.e., the warped wave fronts, causes each beam to converge to a small cloud of points in the aperture plane.

The points are labeled in Fig. 7 according to the information contained in the converged beam. Light converging to o is from the zeroth-diffraction order of each grating and carries no information. Cloud a is the converged beam a, containing a reconstruction of the warpage of wavefront A''. The cloud symmetrically opposite is labeled $-a$ because it is the -1 diffraction order and, therefore, possesses a wave front that is inverted (or the mirror image) with respect to wave front a.[8] Similarly b and $-b$ are comprised of light that reconstructs the wave front warpage of beam b (or B''). For purposes of clarity, light of other diffraction orders, including higher-order and combined-order diffractions, is not labeled.

Optical filtering proceeds as follows. An aperture illustrated by the solid line in Fig. 7 is used first, allowing light from beams a and b to enter the camera. The image formed on the film plane is a contour map of the separation between the two wave fronts; in this case it is $(N_a - N_b + C_1)_p$, where C_1 represents a carrier pattern caused by the angular deviations between beams

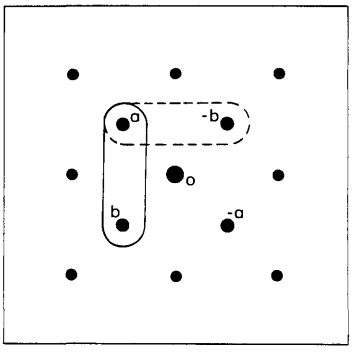

Fig. 7. In the first optical filtering step of Scheme II, numerous diffracted beams fall on the aperture plate of Fig. 5. Beams a and b and subsequently a and $-b$ are admitted into the camera and photographed on separate films.

a and b. This pattern is photographed. Next an aperture is used which allows light from beams a and $-b$ to enter the camera; this aperture is represented by the dashed line in Fig. 7. The interference between these two beams produces a contour map of $[N_a - (-N_b) + C_2]_p$. The pattern is photographed on a separate film.

These steps are repeated for the initial or no-load pattern, and four separate film negatives are produced. Then the corresponding load and no-load negatives are superimposed in registration to produce the moiré patterns of the load-induced fringes exclusively, namely,

$$(N_a - N_b)_{p-i} = (N_a - N_b + C_1)_p - (N_a - N_b + C_1)_i, \quad (6)$$

$$(N_a + N_b)_{p-i} = [N_a - (-N_b) + C_2]_p - [N_a - (-N_b) + C_2]_i. \quad (7)$$

Of course, these yield in-plane and out-of-plane displacements by Eqs. (2) and (3), respectively.

With a final filtering step, as described in Sec. III.A, fringe contrast is enhanced to that of Fig. 8.

The technique of Scheme II will be reviewed in connection with a specific example.

V. Experimental Investigation

A. Specimen and Specimen Grating

An isotropic disk in diametral compression was chosen as a test specimen. The disk was 50.8 mm (2 in.) in diameter and was machined from 9.5-mm (3/8-in.) thick polymethylmethacrylate (PMMA) sheet stock. A phase grating with an aluminized-reflective coating was formed on the specimen surface. This was a crossline grating of f = 600 lines/mm (15,240 lines/in). The grating replication procedure used to form the grating on the specimen surface is described in Refs. 3 and 9.

B. Procedure

The specimen was placed in a loading fixture designed to apply compressive loading while minimizing rigid-body motions of the specimen. The loading frame complete with specimen was placed in the moiré interferometry system illustrated in Fig. 3. Angle α was adjusted to produce a virtual reference grating of 1200 lines/mm (30,480 lines/in). A rotational mismatch between the specimen grating and virtual reference grating was introduced, and orientation of the auxiliary mirror was adjusted resulting in the three beams being converged on the aperture plate as shown in Fig. 6(a).

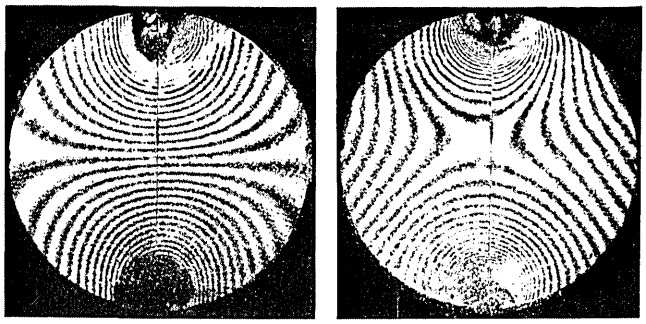

(a) (b)

Fig. 8. Results: patterns of (a) in-plane and (b) out-of-plane displacements for a disk in compression. Slight out-of-plane rigid-body rotation accompanies deformation of the disk.

Angular deviations between the three beams provided $C_x \approx C_{y1} \approx C_{y2} \approx 20$ fringes/mm. All three beams were allowed to enter the camera, and a no-load exposure was made on Film 1. A load was applied to the specimen, and a second exposure was made on a second film, Film 2. All the raw data was acquired in this simple procedure.

After developing, Film 1 was placed in the optical filtering system where two exposures were made. The first consisted of combining beams a and b, as illustrated in Fig. 7, to obtain a fringe pattern of $(N = N_a - N_b + C_1)_i$ and was designated Film 3. The second exposure, on Film 4, was made of the interference pattern between beams a and $-b$ yielding $(N' = N_a + N_b + C_2)_i$. The load negative from the moiré interferometry system was then optically filtered in the same manner, resulting in two corresponding patterns on Films 5 and 6, respectively.

Films 3 and 5 with the no-load and load fringe patterns of the subtractive parameter were superimposed in registration to produce the moiré pattern defined by Eq. (6). It was optically filtered to enhance contrast. This filtered moiré pattern, photographed as Film 7, reveals contours of in-plane displacements accrued between the no-load and load conditions. By Eq. (2), it is a contour map of the U displacement field.

Films 4 and 6, with the no-load and load fringe patterns of the additive parameter, were superimposed in registration to produce the moiré pattern defined by Eq. (7). It was filtered and photographed as Film 8 revealing contours of the load-induced out-of-plane displacements. By Eq. (3), it is a contour map of the W displacement field.

VI. Results and Discussion

The moiré fringe patterns on Films 7 and 8 are shown as Fig. 8(a) and (b), respectively. Figure 8(a) is the easily recognized x-displacement field, the result of the subtractive moiré. Here each fringe represents an in-plane displacement of 1/1200 mm or 0.833 μm (32.8 μin.). The out-of-plane displacement field resulting from the additive moiré is shown in Fig. 8(b). For the experiment conducted here, the green line of an argon laser was used ($\lambda = 514.5$ nm), and $\alpha \approx 18$ deg. Substituting these values into Eq. (3) reveals that sensitivity to out-of-plane displacement was extremely high, namely, 0.132 μm/fringe (5.2 μin./fringe). It should be noted that this is almost twice the sensitivity of normal incidence holographic interferometry.

While the raw data are collected in a very easy and straightforward procedure, numerous optical filtering operations are required for data reduction. It would be attractive to find ways to eliminate the need for Films 3–6, but no direct method seems possible. These intermediate steps extract the sum and difference of wave-front warpages from the raw data before the final step of canceling contributions of the no-load pattern. Optical filtering is seen as a very powerful data manipulation process, and considering its ability to perform the manipulations simultaneously throughout the full field of view, it is an efficient process.

Although the experimental investigation performed for this work consisted of a static test, the simplicity of the technique lends itself to dynamic analyses. One must merely make an exposure containing the no-load information, followed by another exposure (or series of exposures) after initiation of the dynamic event. These exposures can then be processed by optical filtering to determine the change of displacements at the instant of the dynamic exposure.

VII. Conclusions

Effective means have been developed to reveal contour maps of the sum and the difference of wave front warpages of beams emerging from a specimen grating. These depict out-of-plane and in-plane displacement fields, respectively, with very high sensitivities. With Scheme II, only a single photographic record is required for the load condition and another for the no-load condition. Data acquisition is experimentally simple, and the method is amenable to dynamic as well as to static analyses.

This work was supported in part by the National Science Foundation under grant ENG-7824609 with Clifford J. Astill as NSF program director. This support, and the facilities, and the assistance of the staff of the Engineering Science and Mechanics Department of VPI&SU are greatly appreciated.

References

1. M. L. Basehore and D. Post, Exp. Mech. **21,** 331 (1981).
2. D. Post, "Optical Interference for Deformation Measurements—Classical, Holographic, and Moiré Interferometry," *Mechanics of Nondestructive Testing*, W. W. Stinchcomb, Ed. (Plenum, New York, 1980).
3. D. Post, Opt. Eng. **21,** 458 (1982).
4. C. A. Sciammarella, G. Di Chirico, and T. Y. Chang, J. Appl. Mech. 180 (Mar. 1970).
5. W. J. Beranek and A. J. A. Bruinsma, Exp. Mech. **20,** 289 (1980).
6. D. Post and W. A. Baracat, Exp. Mech. **21,** 100 (1981).
7. A. J. Durelli and V. J. Parks, Exp. Mech. **7,** 97 (1967).
8. U. I. Ostrovsky, M. M. Butusov, and G. V. Ostrovskaya, *Interferometry by Holography* (Springer, Berlin, 1980), pp. 186–192.
9. M. L. Basehore, "Moiré Interferometry for Out-of-Plane Displacement Measurements," Ph.D. Dissertation, Virginia Polytechnic Institute and State U. (1981).